Characterization of Short Glass Fiber Filled Polystyrene by Fiber Orientation and Mechanical Properties

Seok Won Lee, Jae Ryoun Youn*

Department of Fiber and Polymer Science, Seoul National University, 56-1, Shinlim-dong, Kwanak-gu, Seoul, Korea

SUMMARY : A quasi-steady state, non-isothermal, compressible, inelastic, and creeping flow of polymer melt into a thin cavity is analyzed to predict fiber orientation states. Modified Cross model and Tait's state equation are adopted to consider shear-thinning behavior and compressibility of the polymer melt. Second order tensors are introduced to describe 3-dimensional fiber orientation. Flow-induced fiber orientation can be predicted by solving the equations of change for the orientation tensor with a suitable closure approximation. The orthotropic closure is applied except for the case of low interaction coefficient. Fiber orientation develops mainly due to shear flow in the skin layer and due to stretching effect in the core layer. It turns out that the compressibility, which induces additional velocity gradients during packing, reduces development of the fiber orientation. Results are dependent upon the magnitude of the interaction coefficient. The larger the interaction coefficient, the smaller the orientation development and the effect of compressibility. To predict orientation dependent mechanical properties, the orientation averaging for an arbitrary orientation is carried out from the properties of a transversely isotropic unit cell. The compressibility reduces the axial modulus and increases the transverse modulus. Opposite trends are observed for thermal expansion coefficients. It is also observed that the consideration of compressibility reduces the overall anisotropy of the molded product. Effects of compressibility on mechanical properties of the parts are reduced as the interaction coefficient becomes larger.

Introduction

Processing of short fiber reinforced composites is of our keen interest because the short fiber composites can retain some advantages of continuous fiber reinforced composites and be produced by injection molding with precision. Injection molding is one of the most widely used processes for the production of short fiber composites. During injection molding, complex flow fields in the cavity are likely to induce fiber orientation. This flow-induced fiber orientation results in anisotropy that affects mechanical properties as well as microscopic structure and final shape of the product. To improve these properties of the part, it is necessary to investigate the procedure of fiber orientation which causes the anisotropy.

After Jeffery's work[1] on the fiber motion in Stokes flow of Newtonian fluid, much research was reported for the prediction of flow induced fiber orientation[2-5]. Since the flow of the

 CCC 1022-1360/99/$ 17.50+.50/0

polymer melt inside the injection mold is not dealt with ease, numerical approaches have been powerful tools[6-15]. So far, the assumption of incompressible polymer melt has been dominant. However, when the cavities are not symmetric or the multi-cavity mold is used, compressibility of the polymer melt affects the velocity profile even in the filling stages of injection molding. While some investigations have been made for the case of pure polymers[16-18], investigations on short fiber reinforced composites have not yet been made.

In this study, the compressibility effect of polymer melt on fiber orientation and resulting mechanical properties was examined. Compressibility of the polymer melt was considered by using Tait's state equation. The modified Cross model was adopted to simulate the viscosity of the polymer melt. Pressure and temperature fields were obtained by the control volume based FEM/FDM hybrid numerical technique. For the prediction of fiber orientation, the equations of change for the second order orientation tensors were solved by the fourth order Runge-Kutta method.

Numerical Analysis

A fiber orientation field inside a cavity is directly related to the flow field. Once the flow field is obtained, variation of the second order orientation tensor can be calculated through a proper procedure. The state, constitutive, continuity, momentum, and energy equations should be solved simultaneously to obtain the flow field. Tucker[19] showed that the flow and the fiber orientation fields can be decoupled as long as the gap inside the cavity is sufficiently small. This is true in most injection molding practices.

Flow Analysis

The coordinate system employed in this study is shown in Fig. 1.

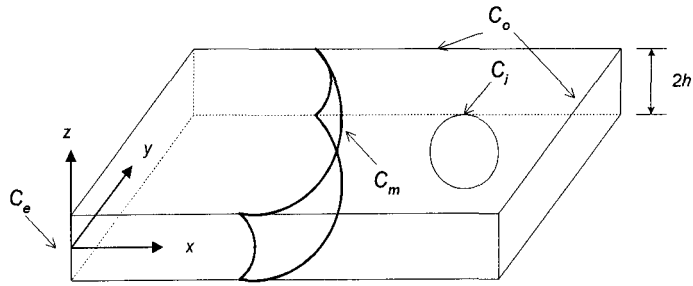

Fig. 1: Schematic presentation of the flow in the mold and the definition of the coordinate system.

With the assumption that the flow inside the cavity is quasi-steady, creeping, non-isothermal, and inelastic, the governing equations can be expressed as follows.

$$\frac{\partial \rho}{\partial t}+\frac{\partial}{\partial x}(\rho u)+\frac{\partial}{\partial y}(\rho v)+\frac{\partial}{\partial z}(\rho w)=0 \qquad \textbf{1}$$

$$0=\frac{\partial}{\partial z}\left(\eta\frac{\partial u}{\partial z}\right)-\frac{\partial p}{\partial x} \qquad \textbf{2}$$

$$0=\frac{\partial}{\partial z}\left(\eta\frac{\partial v}{\partial z}\right)-\frac{\partial p}{\partial y} \qquad \textbf{3}$$

$$\rho C_p\left(\frac{\partial T}{\partial t}+u\frac{\partial T}{\partial x}+v\frac{\partial T}{\partial y}\right)=k\frac{\partial^2 T}{\partial z^2}+\eta\dot{\gamma}^2 \qquad \textbf{4}$$

where x, y, and z are the Cartesian coordinates, u, v, and w are velocity components, p is pressure, T is temperature, ρ is density, C_p is heat capacity, k is thermal conductivity, η is viscosity, and $\dot{\gamma}$ is the magnitude of shear strain rate which is evaluated by the following relation.

$$\dot{\gamma}=\sqrt{\left(\frac{\partial u}{\partial z}\right)^2+\left(\frac{\partial v}{\partial z}\right)^2} \qquad \textbf{5}$$

Variation of the gap thickness of the cavity is handled by using the lubrication approximation[7,9,16,18].

Boundary conditions used for the numerical analysis are given as

$$\begin{aligned} &u=v=w=0 \quad , \quad T=T_w \qquad \text{at} \quad z=h \\ &\frac{\partial u}{\partial z}=\frac{\partial v}{\partial z}=\frac{\partial T}{\partial z}=0 \quad , \quad w=0 \quad \text{at} \quad z=0 \end{aligned} \qquad \textbf{6}$$

where h denotes the half-thickness of the cavity. Integrating Eq. (2) and (3) twice yields u and v.

$$u=-\frac{\partial p}{\partial x}\int_z^h\frac{\tilde{z}}{\eta}d\tilde{z} \qquad \textbf{7}$$

$$v=-\frac{\partial p}{\partial y}\int_z^h\frac{\tilde{z}}{\eta}d\tilde{z} \qquad \textbf{8}$$

where $\tilde{z}$ is a dummy variable.

Mass flow rates can be derived from Eq. (7) and (8).

$$\dot{m}_x=2\int_0^h \rho u\,dz\equiv-2\frac{\partial p}{\partial x}\tilde{S} \qquad \textbf{9}$$

$$\dot{m}_y=2\int_0^h \rho v\,dz\equiv-2\frac{\partial p}{\partial y}\tilde{S} \qquad \textbf{10}$$

where $\widetilde{S}$ is fluidity defined as follows.

$$\widetilde{S} \equiv \int_0^h \rho \int_z^h \frac{\widetilde{z}}{\eta} d\widetilde{z}\, dz \qquad \textbf{11}$$

Integrating Eq. (1) in the thickness direction with the boundary conditions of Eq. (6) yields the following equation.

$$G\frac{\partial p}{\partial t} - \frac{\partial}{\partial x}\left(\widetilde{S}\frac{\partial p}{\partial x}\right) - \frac{\partial}{\partial y}\left(\widetilde{S}\frac{\partial p}{\partial y}\right) = -F \qquad \textbf{12}$$

The term involving the partial time derivative of density is decomposed into G and F because density is a function of pressure and temperature. G and F are defined as follows.

$$G = \int_0^{\chi}\left(\frac{\partial \rho_l}{\partial p}\right)_T dz + \int_{\chi}^{h}\left(\frac{\partial \rho_s}{\partial p}\right)_T dz \qquad \textbf{13}$$

$$F = \int_0^{\chi}\left(\frac{\partial \rho_l}{\partial T}\right)_p \frac{\partial T}{\partial t} dz + \int_{\chi}^{h}\left(\frac{\partial \rho_s}{\partial T}\right)_p \frac{\partial T}{\partial t} dz + (\rho_l - \rho_s)_{z=\chi}\frac{\partial \chi}{\partial t} \qquad \textbf{14}$$

Here, subscripts l and s represent liquid and solid phases, respectively, and χ is the location of the interface. Boundary conditions for the Eq. (12) are

$$\begin{aligned} &\text{at } C_m && p = 0 \\ &\text{at } C_i \text{ or } C_o && \frac{\partial p}{\partial n} = 0 \\ &\text{at } C_e && p = p_e(t) \end{aligned} \qquad \textbf{15}$$

where n denotes outward normal.

The state equation of Tait[16-18] which describes the specific volume of both phases well is employed in this investigation :

$$v(T,p) = \frac{1}{\rho(T,p)} = v_0(T)\left[1 - 0.0894 \ln\left(1 + \frac{p}{B(T)}\right)\right] \qquad \textbf{16}$$

where

$$v_0(T) = \begin{cases} b_{1,l} + b_{2,l}\overline{T} & (T > T_t) \\ b_{1,s} + b_{2,s}\overline{T} & (T < T_t) \end{cases} \qquad \textbf{17}$$

$$B(T) = \begin{cases} b_{3,l}\exp(-b_{4,l}\overline{T}) & (T > T_t) \\ b_{3,s}\exp(-b_{4,s}\overline{T}) & (T < T_t) \end{cases} \qquad \textbf{18}$$

$$\overline{T} \equiv T - b_5 \qquad \textbf{19}$$

$$T_t(p) = b_5 + b_6 p \qquad \textbf{20}$$

The modified Cross model is used for the prediction of non-Newtonian viscosity :

$$\eta = \frac{\eta_0}{1+\left[\frac{\eta_0 \dot{\gamma}}{\tau^*}\right]^{1-n}} \qquad \textbf{21}$$

$$\eta_0 = B\exp\left[\frac{T_b}{T}\right]\exp(\beta p) \qquad \textbf{22}$$

where B, T_b, β, τ^*,and n are material constants.

Linear triangular finite elements as shown in Fig. 2 are used for the calculation of nodal pressures.

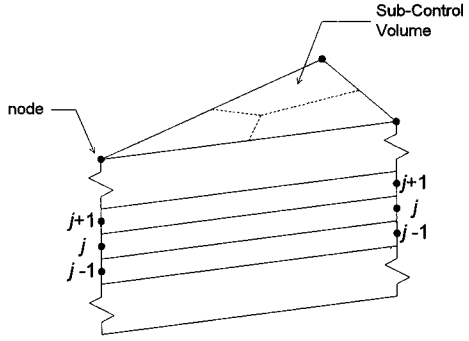

Fig. 2: Linear triangular finite element and finite difference grids in thickness direction, and sub-control volume.

Pressure distribution is assumed to be linear in each element. The Galerkin weighted residual method is applied to Eq. (12) and the first order backward difference for the time derivative of pressure in Eq. (12) is imposed. Each nodal equation is assembled to complete the stiffness matrix. As the result, a nonlinear system of equation is obtained and solved by the iterative substitution method.

Temperatures are calculated at the centroid of each element. The conduction term in Eq. (4) is discretized into the second order central difference (Fig. 2). The backward difference is imposed for the time derivative of temperature in Eq. (4). When convection terms in the planar direction are calculated, an upwinding scheme is used for the numerical stability[16]. Convection terms are evaluated at the previous time step. Equations (4) and (12) are strongly coupled, so they are solved iteratively.

The melt front is advanced by the control volume method. A control volume associated with a node is defined as the sum of the subcontrol volumes (Fig. 2) surrounding the node. The fill factor, f, is defined as the ratio of the amount of the polymers within the control

volume to the amount that the control volume is able to hold. Governing equations apply only to the filled region (f=1). After pressure and temperature fields are obtained, fill factors for the partially filled region ($0<f<1$) are updated. The time step is selected so that the only one control volume needs to be filled at each time step. This is why the control volume method has an advantage in the application of the finite element method to a geometrically complex cavity. Pressure at the gate ($p_e(t)$) is then determined to give the constant volume flow rate which is specified as an input.

Prediction of Fiber Orientation

To predict flow induced fiber orientation, the measure of orientation should be specified first. Orientation tensors are frequently chosen due to their ability to reduce the amount of computation significantly as well as to their normality and symmetry[4]. The second and fourth order orientation tensors are defined as follows.

$$a_{ij} = \int p_i p_j \psi(\boldsymbol{p}) d\boldsymbol{p} \qquad 23$$

$$a_{ijkl} = \int p_i p_j p_k p_l \psi(\boldsymbol{p}) d\boldsymbol{p} \qquad 24$$

where $\boldsymbol{p}$ denotes the unit vector in the fiber direction (Fig. 3) and ψ is the orientation distribution function.

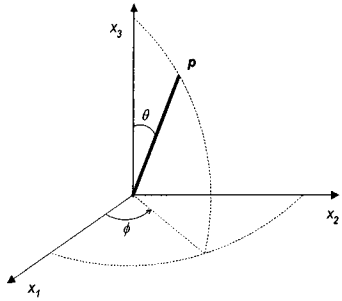

Fig. 3: Position vector of an oriented fiber.

For the prediction of orientation tensors from the flow field, the equation of orientation change for the second order orientation tensor proposed by Advani and Tucker[4] is selected :

$$\begin{aligned}\frac{Da_{ij}}{Dt} &= -\frac{1}{2}(\omega_{ik}a_{kj} - a_{ik}\omega_{kj}) \\ &+ \frac{1}{2}\lambda(\dot{\gamma}_{ik}a_{kj} + a_{ik}\dot{\gamma}_{kj} - 2\dot{\gamma}_{kl}a_{ijkl}) \\ &+ 2C_I\dot{\gamma}(\delta_{ij} - 3a_{ij})\end{aligned} \qquad 25$$

where $\lambda=(r_e^2-1)/(r_e^2+1)$, C_I is the interaction coefficient proposed by Folgar and Tucker[3], and r_e is the aspect ratio of the fiber. The fourth order orientation tensors appear in the above equations and should be expressed in terms of the second order orientation tensors to avoid recurrence. For the purpose, orthotropic closure approximation suggested by Cintra and Tucker[20] is applied. The above equations (23 to 25) are solved by the fourth order Runge-Kutta method with the upwinding scheme for convective terms so that numerical stability should be insured[14].

Prediction of Mechanical Properties

Prediction of mechanical properties is carried out by defining a unit cell in which matrix surrounds a single fiber with the same volume fraction as averaged for the entire composite. The unit cell is assumed to be transversely isotropic. The Halpin-Tsai equation[21] is adopted to predict the modulus of the unit cell :

$$\frac{M}{M_m}=\frac{1+\zeta\xi\phi_f}{1-\xi\phi_f} \qquad \textbf{26}$$

where $$\xi=\frac{(M_f/M_m)-1}{(M_f/M_m)+\zeta} \qquad \textbf{27}$$

M denotes axial modulus, E_1, transverse modulus, E_2, axial shear modulus, G_{12}, or transverse shear modulus, G_{23}. Subscripts f and m denote fiber and matrix, respectively. ϕ_f is the volume fraction of fibers. ζ is given as below :

$$\begin{aligned}\zeta_{E_1}&=2\frac{L}{D}\\ \zeta_{E_2}&=2\\ \zeta_{G_{12}}&=1\\ \zeta_{G_{23}}&=\frac{K_m/G_m}{K_m/G_m+2}\end{aligned} \qquad \textbf{28}$$

L and D is the length and diameter of the fiber. K_m is the bulk modulus and G_m is the shear modulus of the matrix.

Poisson's ratio can be obtained by the rule of mixtures[22].

$$\nu_{12}=\nu_f\phi_f+\nu_m(1-\phi_f) \qquad \textbf{29}$$

ν_{21} and ν_{23} are given by consideration of symmetry constraints as below[22] :

$$\nu_{21}=\nu_{12}\frac{E_2}{E_1} \qquad \textbf{30}$$

$$\nu_{23} = \frac{E_2}{2G_{23}} - 1 \qquad 31$$

Elastic constants obtained by the above equations have the following relationship with the components of the contracted stiffness matrix of a unit cell.

$$\begin{aligned} C_{11} &= \frac{(1-\nu_{23})E_1}{1-\nu_{23}-2\nu_{12}\nu_{21}} \\ C_{22} &= \frac{E_2}{2(1-\nu_{23}-2\nu_{12}\nu_{21})} + G_{23} \\ C_{44} &= G_{23} \\ C_{66} &= G_{12} \\ C_{12} &= \frac{\nu_{21}E_1}{1-\nu_{23}-2\nu_{12}\nu_{21}} \\ C_{23} &= \frac{E_2}{2(1-\nu_{23}-2\nu_{12}\nu_{21})} + G_{23} \end{aligned} \qquad 32$$

Thermal expansion coefficients of the unit cell can be obtained from Schneider's equation[23].

$$\alpha_1 = \alpha_f + \frac{\alpha_m - \alpha_f}{[\phi_f E_f/(1-\phi_f)E_m + 1]} \qquad 33$$

$$\alpha_2 = \alpha_3 = \alpha_m - (\alpha_m - \alpha_f)\times \left(\frac{2(1+\nu_m)(\nu_m{}^2 - 1)C}{(1+1.1\phi_f)/(1.1\phi_f - 1) - \nu_m + 2\nu_m{}^2 C} - \frac{\nu_m E_f / E_m}{1/C + E_f E_m} \right) \qquad 34$$

where C=1.1ϕ_f/(1-1.1ϕ_f).

To predict the mechanical properties of the composite with an arbitrary fiber orientation, orientation averaging is needed from the properties of a unit cell :

$$< \boldsymbol{M} > \equiv \oint \boldsymbol{M}(\boldsymbol{p})\psi(\boldsymbol{p})d\boldsymbol{p} \qquad 35$$

where <***M***> is an averaged tensor property. The following orientation averaging scheme is performed to obtain the thermal expansion coefficient as the second order tensor and the stiffness as the fourth order tensor :

$$< \alpha >_{ij} = A_1\alpha_{ij} + A_2\delta_{ij} \qquad 36$$

$$\begin{aligned} < C >_{ijkl} &= B_1(a_{ijkl}) + B_2(a_{ij}\delta_{kl} + a_{kl}\delta_{ij}) \\ &+ B_3(a_{ik}\delta_{jl} + a_{il}\delta_{jk} + a_{jl}\delta_{ik} + a_{jk}\delta_{il}) \\ &+ B_4(\delta_{ij}\delta_{kl}) + B_5(\delta_{ik}\delta_{jl} + \delta_{il}\delta_{jk}) \end{aligned} \qquad 37$$

A_1, A_2, and B_1 through B_5 are invariants which can be evaluated from the properties of the unit cell :

$$A_1 = \alpha_1 - \alpha_2$$
$$A_2 = \alpha_2 \qquad \textbf{38}$$

$$B_1 = C_{11} + C_{22} - 2C_{12} - 4C_{66}$$
$$B_2 = C_{12} - C_{23}$$
$$B_3 = C_{66} + \frac{1}{2}(C_{23} - C_{22}) \qquad \textbf{39}$$
$$B_4 = C_{23}$$
$$B_5 = \frac{1}{2}(C_{22} - C_{23})$$

The fourth order orientation tensors in the equation (37) are approximated by the orthotropic closure. Finally, stiffness matrix and thermal expansion coefficients within an element are obtained by averaging these quantities as weighted by the thickness of each layer.

Results and Discussion

Figure 4 shows the shape of the cavity and the finite element mesh used in the numerical analysis. The thickness of the cavity is assumed to be 0.2 cm.

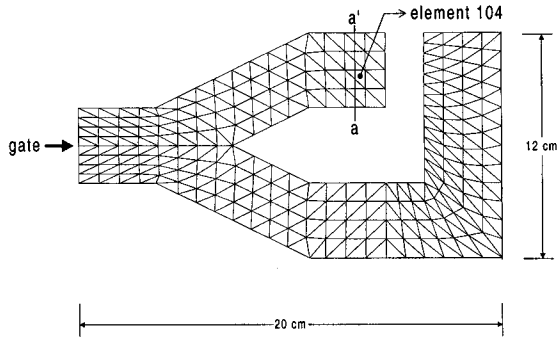

Fig. 4: Mold geometry and finite element mesh configuration.

It is also assumed that glass fiber filled polystyrene is molded. Constants of the modified Cross model[17] for polystyrene are given Table 1.

Table 1. Constants of the modified Cross model for polystyrene.

N	τ (dyne/cm^2)	B (poise)	T_b (K)	β (cm^2/dyne)
0.274	2.31×10^5	3.04×10^{-8}	13300	3.5×10^{-9}

Thermal properties for polystyrene[24] and processing conditions are shown in Table 2.

Table 2. Thermal properties of polystyrene and molding conditions.

k (erg/cm·K·s)	C_p (erg/g·K)	T_{gate} (K)	T_{wall} (K)	Q_{gate} (cm^3/s)
9.8×10^3	2.4×10^7	473	303	35.0

Constants of the Tait's equation for polystyrene are listed in Table 3[17].

Table 3. Constants of the Tait's equation for polystyrene.

$b_{1,l}$ (cm^3/g)	0.988
$b_{2,l}$ ($cm^3/g\cdot K$)	6.10×10^{-4}
$b_{3,l}$ ($dyne/cm^2$)	115.0×10^7
$b_{4,l}$ (K^{-1})	3.66×10^{-3}
$b_{1,s}$ (cm^3/g)	0.988
$b_{2,s}$ ($cm^3/g\cdot K$)	1.49×10^{-4}
$b_{3,s}$ ($dyne/cm^2$)	238.0×10^7
$b_{4,s}$ (K^{-1})	2.10×10^{-3}
b_5 (K)	385.0
b_6 ($cm^2\cdot K/dyne$)	7.8×10^{-7}

Initial random orientation is assumed at the gate and C_I is set to be 0.1, 0.01 or 0.001. Fill time is predicted to be 0.91 sec.

Figures 5 to 7 show orientation ellipses that represent the degree of fiber orientation for incompressible and compressible cases. The ellipse is obtained by the projection of the orientation ellipsoid, which has principal axes in the direction of eigenvectors of the orientation tensor and the magnitude of eigenvalues, into *x-y* plane. Fibers near midplane are aligned perpendicular to the flow direction due to stretching effect while fibers near the wall are oriented parallel to the flow direction due to shear effect. It is found that three distinct regions exist with different fiber orientations. There exist the skin layer near the wall where fibers are oriented in the flow direction, the core layer near the midplane where fibers are oriented transversely, and the transition layer where fibers are rather randomly oriented. These different layers are also experimentally confirmed[11].

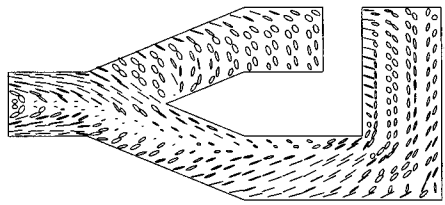

(a)

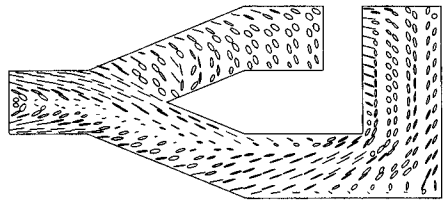

(b)

Fig. 5: Predicted fiber orientation described by the orientation ellipse at z/h=0.0 when C_I=0.01.
(a) compressible case
(b) incompressible case

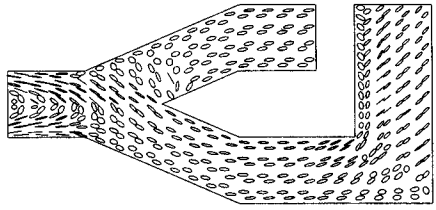

(a)

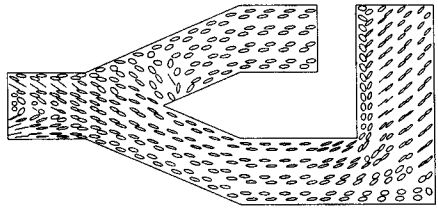

(b)

Fig. 6: Predicted fiber orientation described by the orientation ellipse at z/h=0.3 when C_I=0.01.
(a) compressible case
(b) incompressible case

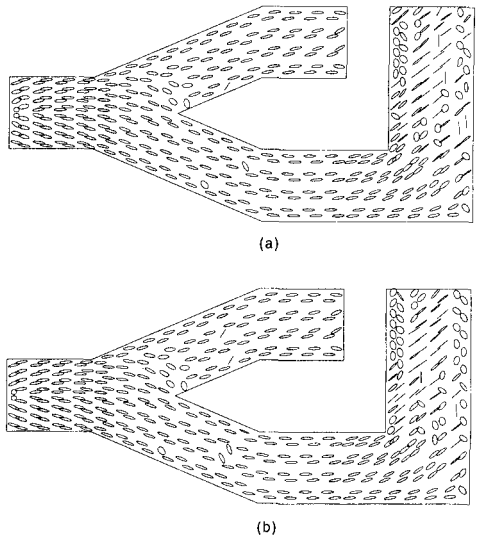

Fig. 7: Predicted fiber orientation described by the orientation ellipse at z/h=0.8 when C_I=0.01.
(a) compressible case
(b) incompressible case

Because of the unsymmetric cavity shape, the polymer melt undergoes compression. The compressibility makes fiber orientation somewhat blunt, which can be seen in Fig.'s 5 and 6. Figure 8 plots maximum eigenvalue of the orientation tensor at the element 104 with respect to the thickness direction. The maximum eigenvalue stands for the degree of orientation in the direction of dominant fiber orientation. It is clearly observed that the compressibility lowers the magnitude of orientation, which is about 4.32% decrease in the maximum eigenvalue. While the effects of the compressibility are significant at the core and transition layers, they are not at the skin layer because fiber orientation is well developed in the region.

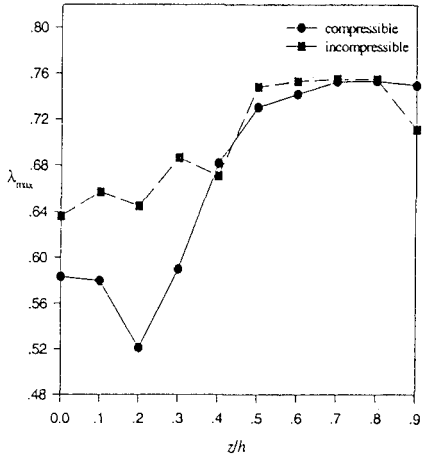

Fig. 8: Predicted maximum eigenvalues of orientation tensors at element 104 in thickness direction at the end of filling when C_I=0.01.

It can be seen from Eq. (23) that factors which determine orientation tensor fields are velocity gradients, because shear rates and vorticity tensors are functions of velocity gradients. Figure 9 shows the gapwise velocity profiles at element 104. The position of element 104 is indicated in Fig. 4. There are significant differences between the two velocity profiles for the compressible case, while little difference is seen for the incompressible case. It should be noticed from the numerical simulation that there are little differences between the velocity profiles for both cases where the effects of the compressibility are not important.

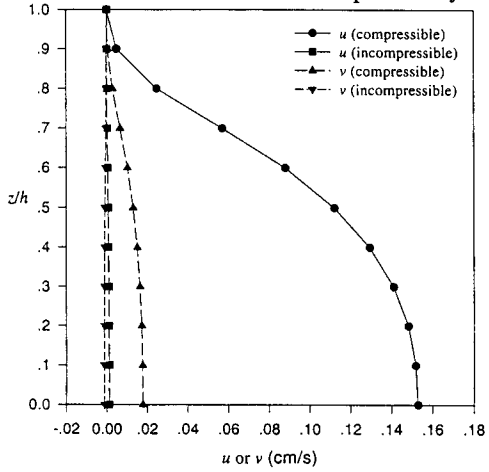

Fig. 9: Gapwise velocity profile after 0.76 seconds at element 104.

In the case of higher C_I of 0.1, the velocity profiles are similar to the previous case, but the fiber orientation is less pronounced. Decrease in the maximum eigenvalue due to the effect of the compressibility is 1.25%, which is lower than the case when $C_I = 0.01$. The higher value of C_I makes orientation more random, so the effect of the compressibility, which also makes orientation random, is not strong. When $C_I = 0.001$, orientation is even more developed than is the case when $C_I = 0.01$. In this case, the orthotropic closure approximation becomes unstable[20], so the hybrid closure[5] is applied. The decrease in the maximum eigenvalue is 5.14%.

Mechanical properties of the fiber and matrix material for prediction of stiffness matrix and thermal expansion coefficients are given in Table 4.

Table 4. Physical properties of the glass fiber and polystyrene matrix.

L (cm)	D (μm)	E_f (MPa)	ν_f	α_f (K^{-1})	E_m (MPa)	ν_m	α_m (K^{-1})	ϕ_f (%)
0.1	10	73,000	0.25	5×10^{-6}	3,200	0.33	7×10^{-5}	21

Predicted axial moduli(E_1) are plotted in Fig. 10 at the section a-a' where the effects of the compressibility are likely to be present. Moduli near the side walls are higher than those in the middle due to axial alignment of fibers by the shear effect near the side walls. The effects of the compressibility lower axial moduli by about 2.11%. Figure 11 shows predicted transverse moduli(E_2) at the section a-a'. They are higher in the middle rather than near the side walls because of the fact that the compressibility, which makes fiber orientation random, forces fibers to align in the transverse direction. Thus, the difference between axial and transverse moduli becomes smaller when the compressibility of the polymer melt is considered.

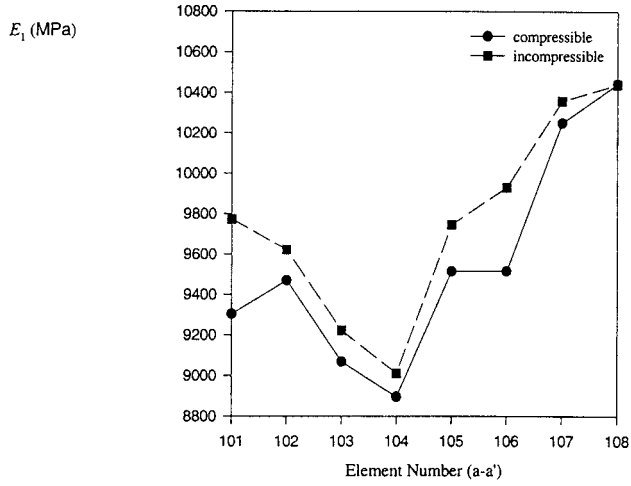

Fig. 10: Predicted axial modulus, E_1, across the section a-a' when C_f=0.01.

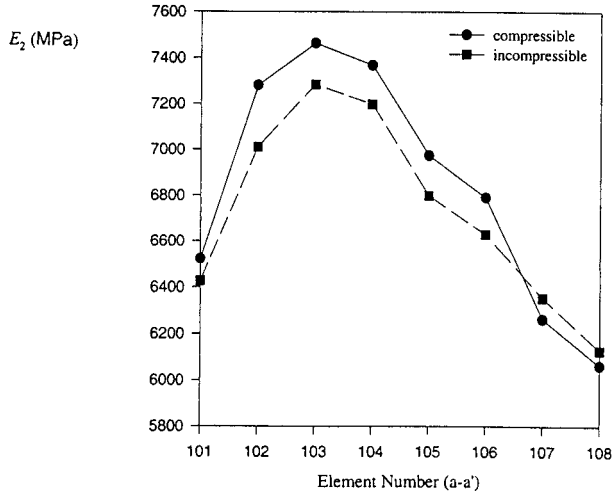

Fig. 11: Predicted transverse modulus, E_2, across the section a-a' when C_f=0.01.

Opposite results to the case of moduli are observed in the case of thermal expansion coefficients because the glass fiber has smaller thermal expansion coefficient than matrix. Predicted axial thermal expansion coefficients(α_{11}) at the section a-a' are plotted in Fig. 12. They are about 2.81% higher in the compressible case than the incompressible case, which is opposite to the prediction of moduli. Transverse thermal expansion coefficients(α_{22}) at the section a-a' are plotted in Fig. 13. There is about a 1.51% decrease from the incompressible as compared to the compressible case. It is expected that more thermal expansion in the transverse direction will happen because thermal expansion coefficients in the transverse

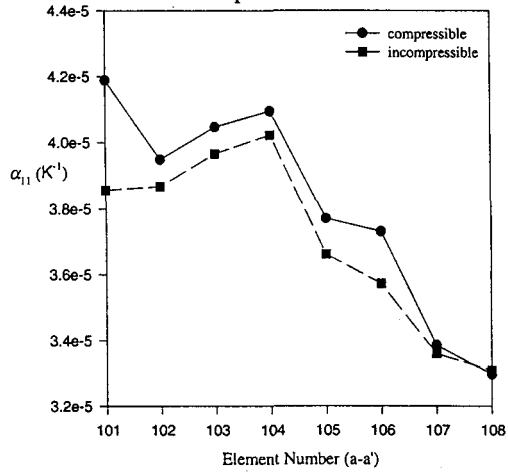

Fig. 12: Predicted axial thermal expansion coefficient, α_{11}, across the section a-a' when C_f=0.01.

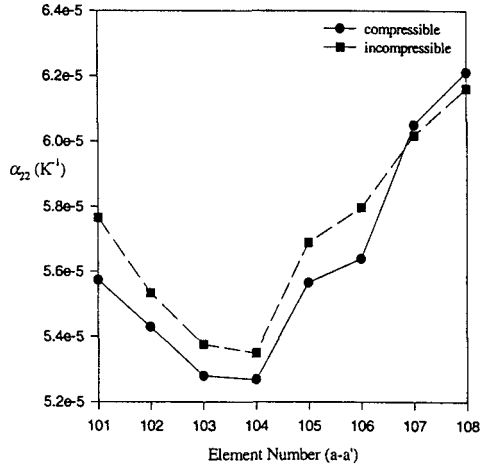

Fig. 13: Predicted transverse thermal expansion coefficient, α_{22}, across the section a-a' when C_f=0.01.

direction are higher than those in the axial direction. Therefore, shrinkage due to solidification is likely to be lower or more homogeneous at the regions where the polymer melt is compressed.

In the case of C_I of 0.1, axial moduli decrease by about 0.50% while transverse moduli increase by about 1.51% when the compressibility is considred. Fiber orientation is not so randomized as is the case when C_I= 0.01. When C_I= 0.001, the difference in moduli between the compressible and incompressible cases is more pronounced. Axial moduli decrease by 3.36%, while transverse moduli increase by 3.33%. Effects of the compressibility, which reduces the degree of orientation, increase as the value of C_I decreases.

Conclusions

Effects of compressibility of the polymer melt on fiber orientation, elastic moduli, and thermal expansion coefficients of the short fiber composites are investigated. The Tait's state equation was employed to consider the compressibility of the polymer melt and the modified Cross model was adopted for flow analysis in the mold cavity. Second order orientation tensors were successfully used to predict the flow induced fiber alignment by solving the equations of change for orientation tensor with a proper closure approximation. It was shown that the compressibility of the polymer melt reduces development of the fiber orientation in the cavity during the packing stage. Anisotropy in mechanical properties and thermal expansion was predicted based on the results of compressible non-isothermal flow and fiber orientation simulations.

Acknowledgement

This study is partially supported by the Korean Science and Engineering Foundation. The authors are grateful for the support.

References

1. G. B. Jeffery, *Proc. Roy. Soc. Ser. A*, **102**, 161 (1923)
2. R. C. Givler, M. J. Crochet, R. B. Pipes, *J. Compos. Mater.*, **17**, 330 (1983)
3. F. Folgar, C. L. Tucker III, *J. Reinf. Plast. Compos.*, **3**, 98 (1984)
4. S. G. Advani, C. L. Tucker III, *J. Rheol.*, **31**, 751 (1987)
5. S. G. Advani, C. L. Tucker III, *J. Rheol.*, **34**, 367 (1990)
6. W. C. Jackson, S. G. Advani, C. L. Tucker III, *J. Compos. Mater.*, **20**, 539 (1986)

7. M. C. Altan, S. Subbiah, S. I. Güçeri, R. B. Pipes, *Polym. Eng. Sci.*, **30**, 848 (1990)
8. S. G. Advani, C. L. Tucker III, *Polym. Compos.*, **11**, 164 (1990)
9. H. Henry De Frahan, V. Verleye, F. Dupret, M. J. Crochet, *Polym. Eng. Sci.*, **32**, 254 (1992)
10. R. S. Bay, C. L. Tucker III, *Polym. Compos.*, **13**, 317 (1992)
11. R. S. Bay, C. L. Tucker III, *Polym. Compos.*, **13**, 332 (1992)
12. S. Ranganathan, S. G. Advani, *J. Non-Newt. Fluid Mech.*, **47**, 107 (1993)
13. J. Ko, J. R. Youn, *Polym. Compos.*, **16**, 114 (1995)
14. J. Ko, *PhD Thesis*, Kaist, 1994
15. S. T. Chung, T. H. Kwon, *Polym. Eng. Sci.*, **35**, 604 (1995)
16. H. H. Chiang, C. A. Hieber, K. K. Wang, *Polym. Eng. Sci.*, **31**, 116 (1991)
17. H. H. Chiang, C. A. Hieber, K. K. Wang, *Polym. Eng. Sci.*, **31**, 125 (1991)
18. B. S. Chen, W. H. Liu, *Polym. Eng. Sci.*, **34**, 835 (1994)
19. C. L. Tucker III, *J. Non-Newt. Fluid Mech.*, **39**, 239 (1991)
20. J. S. Cintra Jr., C. L. Tucker III, *J. Rheol.*, **39**, 1095 (1995)
21. J. C. Halpin, J. L. Kardos, *Polym. Eng. Sci.*, **16**, 344 (1976)
22. R. M. Jones, *Mechanics of Composite Materials*, McGraw-Hill, London 1975, p. 37
23. W. Schneider, *Kunststoffe*, **61**, 273 (1971)
24. Y. Kuo, M. R. Kamal, *AIChE J.*, **22**, 661 (1976)